Classification and detection of Fundus Images and Eye Diseases using Deep Learning Techniques

Kande Archana[1]
Assistant Professor
Department of CSE
Malla Reddy College of Engineering
Hyderabad, Telangana, India

Vadlamani Veerabhadram[2]
Associate Professor
Department of CSE
CVR College of Engineering
Hyderabad, Telangana, India

Dr Maram Ashok[3]
Professor
Department of CSE
Malla Reddy College of Engineering
Hyderabad, Telangana, India

Abstract: Deep learning algorithms enable a variety of methods for the diagnosis of eye conditions, including age-related macular degeneration (AMD), glaucoma (GLC), and diabetic retinanopathy (DR). A few recent research contrasted data from healthy participants with the examination of a few main disorders. However, up until now, computer-aided methods have not been able to identify numerous main eye disorders, such as AMD, GLC, and DR, concurrently. Four types of fundus image classification were present, but only two pairs of healthy and eye-diseased groups were the subject of high-performance outcome studies. Gaining a deeper understanding of multi-category classification of Optimal residual deep neural networks and effective picture preparation methods, like constricting the region of interest, were employed in the fundus photos. Data augmentation and iso-luminance plane contrast-limited adaptive histogram equalization. Utilizing them for the categorization of three ocular conditions from presently accessible public datasets, we attained average and peak accuracy rates of 85.79% and 91.16%, respectively. For healthy eyes, GLC, AMD, and DR patients, the specificities were 90.06%, 99.63%, 99.82%, and 91.90%, respectively. Improved specificity results could warn patients of eye disorders early on and help them avoid losing their vision. As a successful pilot research of classification for the three most common eye disorders, this study shows a potential use of a multi-categorical deep neural network technique that may be employed for future assistive devices in computer-aided clinical applications.

Keywords: Multi-categorical classification, deep neural networks, glaucoma, age-related macular degeneration; diabetic retinopathy.

1. INTRODUCTION

The primary causes of vision loss and blindness worldwide are diabetic retinopathy (DR), glaucoma (GLC), and age-related macular degeneration (AMD). These three conditions are the subject of our investigation. Diabetes mellitus, the most prevalent cause of vision loss and blindness in adults, is the cause of diabetic retinopathy (DR) [1,2]. Global diabetes prevalence was predicted to increase from 2.8% (171 million) to 4.4% (3.4%) by 2030 [3], with an additional 195 million individuals expected to have diabetes-related disorders (DR) [4-6]. Within the following 20 years, it was anticipated that nearly all individuals with type 1 diabetes and more than 60% with type 2 diabetes would get DR [7]. In the following 15 years, these diabetic patients were predicted to account for roughly 10% of vision loss and 2% of blindness [8]. Although the reported patients have grown gradually, it was anticipated that they would develop quickly. A report from the beginning of the twenty-first century states that the incidence of diabetes mellitus has doubled in the US and climbed three to five times in countries like India, Indonesia, China, Korea, and Thailand [9]. Both industrialized and emerging nations saw the rise of DR. The impact of differential pressure in intraocular lenses is the second most frequent cause of vision loss, or GLC. 6.7 million of the 66.8 million individuals who had primary GLC in 2000 also experienced bilateral blindness [10]. About 60.5 million GLC patients worldwide were affected by this disease by 2010, making it the second most common cause of vision loss and blindness [11]. Both the bending of the optic nerve head and the damage to the optic nerve's origin can be detected in fundus photography photos. AMD, which poses a serious threat in developed nations, is the third most prevalent cause of vision loss and blindness. Even if DR and GLC were more common, AMD incidence has increased in those over 60, and it has been estimated that AMD alone accounts for 8.7% of blindness globally, primarily in wealthy nations [12–20]. Those who experienced AMD have undoubtedly faced challenges in their lives because vision is one of the five fundamental human senses. In addition, the second sensitive and important nerve among the twelve cranial nerves is the optic nerve, also known as the nerve of sight.

Experts or medical professionals use a variety of methods to diagnose eye conditions; two common ones are fundus photography and optical coherence tomography, which produces a cross-sectional image. In addition to the eye, optical coherence tomography has been crucial in the diagnosis of other organs like the brain. Many researchers, including Hwang et al. [21], Bussel et al. [22], and Lee et al. [23], had examined the cross-sectional

pictures of the eye damaged by DR, GLC, and AMD using this technique; nevertheless, the techniques had certain drawbacks.

Photographs from fundus photography researchers have shown a significant amount of interest in studying the inner eye using a customized camera. Several eye conditions can be identified using the same photograph, including the three in this investigation. The different fundus photography methods can be divided into three categories: fluorescein angiographic, mydriatic, and non-mydriatic. These methods involve using fluorescent or indocyanine green dyes to examine the retina, as well as using pupil dilation and imaging without dilation to examine the choroid or blood flow. This study aims to classify eye illnesses by combining fundus pictures from multiple open-source datasets.

We guarantee that this work will be a pioneer in future research. The current study employs a feedforward neural network to identify multiple eye disorders using fundus photos. Numerous research, including those by Qummar et al., have applied deep learning techniques in the field of DR detection. [24] developed an automatic DR detection system for retinal images using an ensemble approach, and Mateen et al. [25] developed a DR image classification system using a combination of Gaussian mixture model, Visual Geometry Group (VGG) networks, singular value decomposition, and principle component analysis. A few research have combined ensemble and neural network approaches to GLC identification; Singh et al. [26] developed an autonomous GLC diagnostic system by combining a deep learning ensemble with feature selection techniques. In the study by Tan et al. [27], a suggested computer-aided diagnosis system based on a customized convolutional neural network offered second opinions to help ophthalmologists in AMD diagnosis. Numerous studies on computer-aided diagnosis have been published; these studies may provide ophthalmologists with tools to help with the screening and diagnosis of eye diseases.

The structure of this document is as follows. A overview of the literature on eye diseases is presented in Section 2. We detail how we acquired our data in Section 3. The methods used for preprocessing and processing Section 4 describes the methods used in the paper. Here are our classification findings in Section 5. Section 6 provides a discussion and a conclusion.

2. RELATED WORK

Numerous research have contributed significantly to the direction of investigations on the various methods used in the identification of eye diseases. In this paper, we used a deep convolutional neural network (DNN) to examine classification. The most popular methods for utilizing fundus photography for illness screening and detection were DNN, classical machine learning, and feature extraction with an ensemble. As was already indicated, earlier research [24–27] offered opportunities for diagnosing and categorizing eye disorders. The current study, however, focuses on one method—DNN—that has been investigated recently by numerous researchers in order to give the classification of a variety of eye illnesses.

Many neural networks have been used to autonomously diagnose eye disorders, including new, pre-trained convolutional and meta-cognitive neural networks. For DR screening. A neural network diagnostic approach with 88.40% sensitivity and 83.50% specificity was proposed by Gardner et al. [28]; a novel meta-cognitive neural network that monitored and controlled a cognitive neural network was proposed by Banu et al. [29] and produced 100% accuracy, sensitivity, and specificity. The optic disc was one of the most important characteristics of GLC identification in this study, and this performance was attained by removing it from fundus images utilizing the methods of "robust spatial kernel fuzzy c-means" before the meta-cognitive neural network classifier. In contrast, a support vector machine model for GLC detection was proposed by Raghavendra et al. [30]. Using a 26-feature classification strategy, their method produced maximum results of 93.62%, 87.50%, and 95.80%, respectively, across a public dataset. Furthermore, a different study [31] suggested an 18-layer neural network model to identify GLC the method was very different from earlier neural network models, producing accuracy, sensitivity, and specificity of 98.13%, 98.00%, and 98.30%, respectively.

Two experimental studies are representative of the AMD detection field. Burlina et al. [32] proposed a pre-trained convolutional neural network model that achieved peak accuracy, sensitivity, and specificity of 95.00%, 96.40%, and 95.60%, respectively. Lee et al. [23] proposed a method with a 21-layer neural network that yielded accuracy, peak sensitivity, and peak specificity of 93.45%, 92.64%, and 93.69%, respectively. At the feedforward step, a large neural network would be able to automatically identify several eye disorders without producing classification results that overlap. As a result, it could be able to identify these illnesses earlier and lessen the amount of blindness and visual loss they cause. In their pilot research, Choi et al. [33] employed a deep neural network (VGG-19). When applied to images from the Structured Analysis of the Retina (STARE) database, the technique of transfer learning with a random forest yielded a peak accuracy of 72.8% for three-class early disease screening among normal retina (NR), background DR, and dry AMD. Furthermore, using the

same model structure, five-class eye illness classification—NR, background DR, proliferative DR, dry AMD, and wet AMD—achieved a maximal accuracy of 59.1%. This performance was not good enough for a tiny database. However, this groundbreaking study demonstrated that using a 19-layer neural network to analyze a 397-file database including 14 illness categories could be able to produce a result that is satisfactory. The present work was inspired by the documented capabilities of vast neural networks. Examination of this intriguing potential for multi-eye disease diagnosis using a deeper pre-trained neural network on publicly accessible web datasets.

3. PROPOSED METHODOLOGIES

Ophthalmologists will greatly benefit from automatic classification of the three most prevalent retinal fundus illnesses, which will aid in the early and affordable diagnosis of eye problems. The training and testing parts of the suggested method consist of two stages: preprocessing the data and categorizing retinal images. Fig. 6 illustrates the suggested method. First, the reducing region of interest, iso-luminance plane contrast limited adaptive histogram equalization, and other preprocessing steps were applied to each dataset. data augmentation with k-fold cross-validation. Second, training settings were applied to each training set that emerged from the pre-processing phase in order to generate a learned weight for every dataset. Lastly, To produce the testing results of the eye-disease classifications, each testing set was forecasted using the learned weight generated during the training phase.

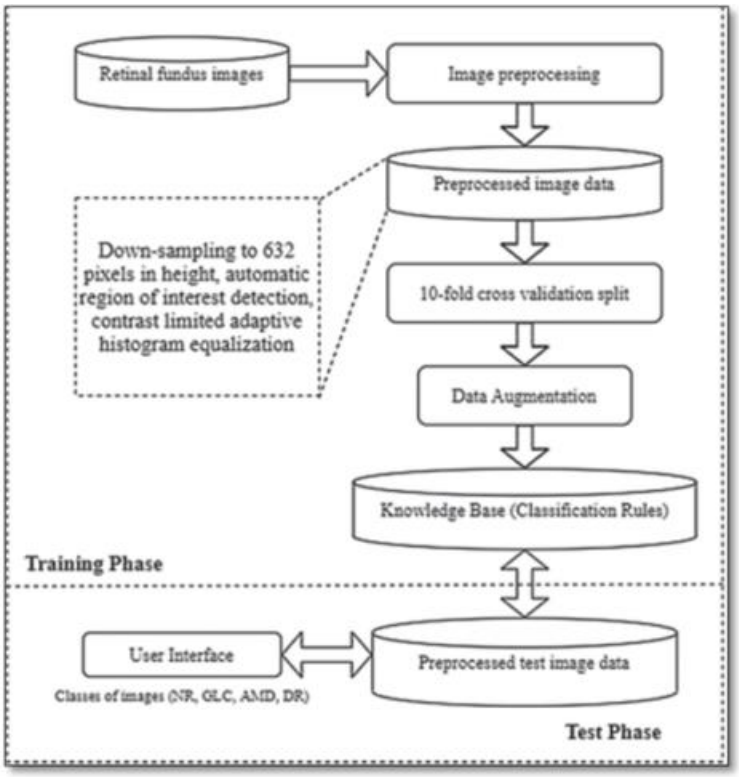

Figure 6 - Eye disease evaluation process

3.1 Pre-Processing

Prior to training our model, we used many picture normalizing techniques. Different researchers approached the preprocessing of their images in different ways. In order to standardize the original fundus images across the datasets, we reduced their region of interest in this work. This was automatically carried out, with the blue channel serving as a complimentary layer and the red and green channels having thresholds of 25 and 13, respectively. The following represents the coordinates for decreasing the region of interest, where imax and jmax denote the width and height of the image:

$$ROI = \begin{cases} (X_1, Y_1) = \max\left(\forall r_{i,j} < 25\right) \cup \left(\forall g_{i,j} < 13\right) & for\ \forall (i,j) \in \left[0, \frac{(i,j)_{\max}}{2}\right] \\ (X_2, Y_2) = \min\left(\forall r_{i,j} < 25\right) \cup \left(\forall g_{i,j} < 13\right) & for\ \forall (i,j) \in \left[\frac{(i,j)_{\max}}{2}, (i,j)_{\max}\right] \end{cases} \quad (1)$$

We also used a different preprocessing method that we named ISOL-CLAHE. The application of contrast-limited adaptive histogram equalization (CLAHE) on an isoluminant plane is known as ISOL-CLAHE. We adjusted this method for our retinal fundus images within an isoluminant plane, as stated by Han et al. [41]. The isoluminant plane histogram equalization enhanced the linear cumulative distribution function's lowest mean absolute error rate. Between earlier research on independent RGB histogram equalization [41–43]. Three-dimensional CLAHE was performed on each of the original image files, which were spread throughout eight child subdirectories and four parent folders (NR, GLC, AMD, and DR). Using software from an open-source library, the photos were transformed to a color space prescribed by the International Commission on Illumination (abbreviated CIELAB in French) in order to extract lightness [44]. CLAHE with a scaling grid kernel size of eight and a clip limit of 1.5 was then resized to 384 × 384 pixels. ROI shrink and ISOL-CLAHE implementation are shown in Fig. 7.

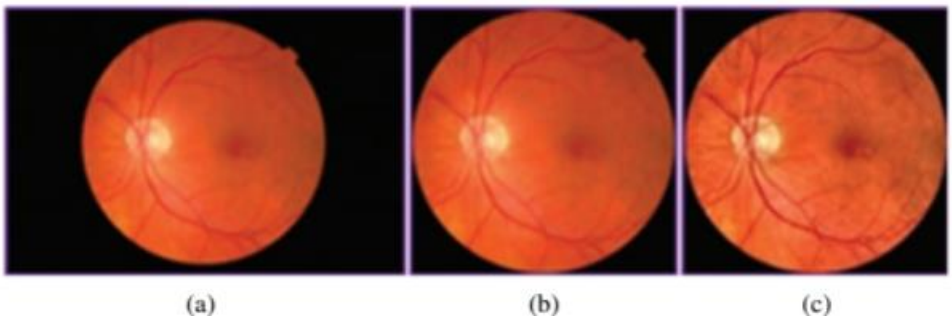

Figure 7: Shrinking region of interest (ROI), (a) The original image with its original size. (b) The ROI shrinking image. (c) The ISOL-CLAHE image

Breiman et al. [45] found that in models with more characteristics, K-fold cross-validation in its tenfold variant outperformed leave-one-out, twofold, and fivefold cross-validation. According to Ron Kohavi [46], bootstrapping with a smaller variance but an exceptionally big bias was not as effective as stratified tenfold cross-validation, which outperformed twofold and fivefold cross-validation. To avoid bias from the data preparation, we employed stratified tenfold cross-validation with data shuffling for the fundus image categorization in the current investigation, as described by [47]. Three portions totaling 80%, 10%, and 10% of the images were taken from the entire dataset for testing, validating, and experimental training, respectively.

One way to increase datasets without generating bogus images is termed data augmenta- tion. There were different numbers of photos for each category of sickness in the gathered dataset. Suddenly, a An image underwent many transformations, including an 8-degree rotation, a 25% brightness adjustment, a 20% magnification, and a horizontal reflection. Because there were numerous NR and DR images and very few AMD images, this resulted in a balanced training and testing dataset of up to 9400 images for the entire combined dataset experiment, preventing performance discrepancies. We did not employ the data augmentation method's common changes, like shear or shifts in height or width. Usually, the participant faced forward when an ophthalmologist took the fundus photograph. Shear range may thus not be a possibility in this process. Similar to this, every naturally occurring structure, such as an optic disc, a macula, and blood vessels, should be present in the fundus image. For this reason, we decided not to apply in case doing so would unintentionally remove one of these features. Figure 8 displays a few instances of data augmentation on a MESSIDOR dataset.

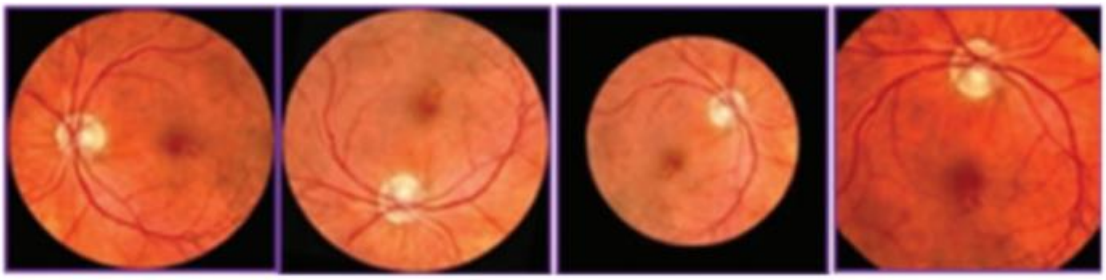

Figure 8: Illustrations of data augmentation from a MESSIDOR image-set. (a) The original image from ISOL-CLAHE. (b) An augmented image with +25% brightness and 80◦ rotation. (c) An augmented image with +25% brightness, 20% zoom-out, horizontal flip, and 40◦ rotation. (d) An augmented image with 25% brightness, 20% zoom-in, horizontal flip, and 80◦ rotation

3.2 Model Architectures and Settings

Deep neural networks known as Residual Networks (ResNets) were so called because of their residual state [48]. By employing a shortcut link, this kind of network made a breakthrough over pointless convolutional layer blocks [49]. We used three residual network (ResNet) architectures: ResNet-50, ResNet-101, and ResNet-152. These three ResNet architectures each had 50, 101, and 152 weight layers with 25, 610, 216, 44, 654, 504, and 60, 344, 232 total parameters. These models had 224 × 224 × 3 input and 1,000 fully connected Softmax regression classes as their initial shapes. For this investigation, we optimized the input shape to 384 × 384 × 3, and the result was a four-class fully linked Softmax regression prediction probability. The Visual Geometry Group presented two networks, VGG-16 and VGG-19, with a total of 138 million and 144 million parameters, respectively, made up of 16 and 19 weight layers [50]. Both the original and modified input and output shapes that we employed in this investigation were exactly the same as those found in ResNets.

In order to obtain the most accurate form possible, neural network optimizers were crucial in helping to choose and adjust these weights. Loss functions helped the optimizers make the proper decisions. In comparison to the adaptive gradient algorithm optimizer that came before it, an adaptive gradient extension optimizer called Adadelta enhanced learning robustness and learning rate variation [48]. According to Zeiler [51], this optimizer outperformed a number of rivals, including momentum and stochastic gradient descent optimizers, in terms of test error rate. We employed a categorical cross-entropy loss function and an adaptive gradient extension optimizer with a learning rate of 0.001.

There were numerous methods available to stop the network from overfitting. Early-stopping is an effective method that monitors the validation error rate during training and ends the procedure if the validation error did not decrease within a predetermined period of epochs, or "patience" [48]. The likelihood of overfitting could be ascertained with an ideal drop-out rate. Gal et al. [52] suggested combining early-stopping with drop-out rate optimization in order to reduce test mistake rates. In the current work, we employed an early-stopping function with a dropout rate of 0.05 for the best prevention of overfitting, a patience of 20 epochs, and a minimum increment for the validation-loss of 0.001.

We used the tools TensorFlow [53] and Scikit-Learn [54] to train and assess the suggested architecture deep neural network models in order to carry out the classification. We applied the following strategy to our dual-core system configuration: 2.2 GHz Intel Xeon Silver 4114 CPUs, 12 x 16 GB DIMM DDR4 Synchronous RAMs, 3 x 512 GB Samsung 970 NVMe M.2 SSDs, and 3 x NVIDIA TITAN RTX GPUs with 24 GB GDDR6@1770 MHz–4608 Compute Unified Device Architecture (CUDA) cores are all included in this configuration.

4. REUSLTS AND DISCUSSION

We acquired intriguing performance statistics on data augmentation using a ResNet with a depth of 50-layer layers after evaluating the four-class eye-disease classification system utilizing various DNN model designs. As previously stated, noise from non-GLC photos was included in the NOISE-STRESS test dataset. A neural network was considered to be a great classifier for multi-class categorization if it performed better than the

others. It may have outperformed it, though, because it overfitted the noise data, which would have led to issues with multi-class detection. The ResNet-50 achieved average accuracy and sensitivities of 73.16%, 18.13%, 53.33%, and 79.00% for NR, GLC, AMD, and DR with the 2335 source pictures correspondingly.

Additionally, the specificities for these four classes were 70.45%, 98.74%, 99.73%, and 81.77%, respectively. When it came to data augmentation, the ResNet-50 model outperformed the VGG networks or their deeper siblings, the ResNet-101 and ResNet-152 models. On average, the ResNet-50 model achieved 76.71% with data augmentation, and its sensitivities for NR, GLC, AMD, and DR were 45.40%, 83.96%, 98.00%, and 79.49%, respectively. The specificities for these four classes were 88.51%, 91.99%, 99.26%, and 89.19%, respectively. Given these performance rates, it may be reasonable to conclude that the datasets' data augmentation resulted in generalization across the models. Tab 4 displays the NOISE-STRESS dataset test results.

Table 4: Full combined dataset (NOISE-STRESS) test result

	Accuracy	NR (%)		GLC (%)		AMD (%)		DR (%)	
		Sens.	Spec.	Sens.	Spec.	Sens.	Spec.	Sens.	Spec.
ResNet-50	73.12	77.06	70.45	18.13	98.74	53.33	99.73	79.00	81.77
ResNet-101	69.65	73.28	68.13	19.38	98.28	40.00	99.51	75.78	79.01
ResNet-152	63.59	64.03	67.95	3.13	99.91	23.33	99.78	76.44	66.31
ResNet-50 (augmentation)	76.71	45.40	88.51	83.96	91.99	98.00	99.26	79.49	89.19
ResNet-101 (augmentation)	75.06	38.89	89.02	82.72	90.78	97.32	98.79	81.32	88.16
ResNet-152 (augmentation)	74.54	37.74	89.19	82.21	90.38	97.96	98.10	80.26	88.38
VGG-16 (augmentation)	75.78	41.32	89.52	86.60	91.55	95.15	98.77	80.04	87.87
VGG-19 (augmentation)	74.66	36.89	90.45	84.64	91.65	93.06	98.61	84.04	85.50

∗Sens. and Spec. are the performance sensitivity and specificity, respectively.

Testing using the NOISE dataset revealed that the reduction in data enhanced classification performance and produced a greater degree of detection generalization models. The sensitivities for NR, GLC, AMD, and DR were 57.23%, 83.11%, 99.53%, and 81.19%, respectively, while the average accuracy was 80.27%. These four groups had specificities of 89.21%, 92.03%, 99.02%, and 93.43%, in that order. Higher performance was achieved by reducing the stress of information generalization throughout the CNN by excluding mild and moderate DR pictures from the NOISE-STRESS dataset. This test was an investigation into what would happen if there were less stress data using a neural network. Since stress data for DR and other illness types are typically prevalent in the open-access dataset, we have included a STRESS result including those data in this paragraph. The NOISE-STRESS, NOISE, and STRESS dataset test results are displayed in Tab 5.

Table 5: NOISE-STRESS, NOISE, and STRESS dataset test result

	Accuracy	NR (%)		GLC (%)		AMD (%)		DR (%)	
		Sens.	Spec.	Sens.	Spec.	Sens.	Spec.	Sens.	Spec.
ResNet-50	73.12	77.06	70.45	18.13	98.74	53.33	99.73	79.00	81.77
ResNet-50 (Aug.) (NOISE-STRESS)	76.71	45.40	88.51	83.96	91.99	98.00	99.26	79.49	89.19
ResNet-50 (Aug.) (NOISE)	80.27	57.23	89.21	83.11	92.03	99.53	99.02	81.19	93.43
ResNet-50 (Aug.) (STRESS)	85.79	75.52	90.28	97.90	99.54	99.06	99.15	70.66	92.08

∗Aug. is an abbreviation of “augmentation.”

The average accuracy of the ResNet-50 model with data balancing was 85.79%, while the sensitivities of NR, GLC, AMD, and DR were 75.52%, 97.90%, 99.06%, and 70.66%, respectively, after removing non-GLC images from the NOISE-STRESS dataset. The rates of specificities for the four classes were 92.08%, 99.54%,

99.15%, and 90.28%, in that order. Better caution for patients in the early stages of eye disorders is suggested by the improved specificity performances when compared to those using the NOISE-STRESS dataset. The outcomes of k-fold cross-validation testing for non-GLC, mild, and moderate DR. The omitted dataset's max accuracy for the four-class eye illness classification trial was 91.16%. The 50-layer ResNet's average accuracy using tenfold cross-validation was 85.79%. The outcomes of evaluating different k-fold cross-validations using the STRESS dataset are displayed in Tab. 6.

Table 6: Individual fold accuracy from STRESS dataset

	Fold 0	Fold 1	Fold 2	Fold 3	Fold 4	Fold 5	Fold 6	Fold 7	Fold 8	Fold 9	Average	Standard deviation
ResNet-50 accuracy %)	86.05	91.16	88.67	86.88	89.50	82.04	80.11	85.77	82.60	85.08	85.79	±3.48

5. DISCUSSION AND CONCLUSION

As Perez et al. [55] pointed out, data augmentation was crucial to data generalization with a dataset since it increased validation accuracy. However, we also saw impressive testing performances with these fundus photos as a consequence of data augmentation in the Results, section 4. We also noticed, from the entire combined testing dataset, that the ResNet-50 model performed better at classifying eye diseases when paired with data augmentation than other competing models. We believe that the ResNet-50 model could extract as many features as possible from an image with a resolution of 384 × 384 pixels, given the available depth. Furthermore, the networks may be able to learn everything that fundus images may teach them thanks to their residual properties. The nodes in deeper residual models may get an excessive number of features, which could lead to a small amount of overfitting.

To examine the performance gain resulting from utilizing less stress data, we removed the mild and moderate DR images from our training and testing dataset (see Results, Subsection 5.2). Our hypothesis that higher performances were achieved with less challenging data was validated by the small improvement observed with the NOISE dataset. As anticipated, the accuracy of this experiment was 80.27%, while the prior experiment's accuracy was 76.71%.

We created a dataset in our experimental sequence to assess noise tolerance. Consequently, the STRESS dataset yielded an accuracy of 85.79% (Result, Subsection 5.3). 482 of the 650 photos in total were non-GLC photos, either NR or non-GLC from ORIGAlight. After removing the 40% of noisy data from our NR data, the experiment's performance dramatically improved. Furthermore, as anticipated, the stress inclusion of the mild and moderate DR images from the MESSIDOR dataset slightly affected overall performances. To improve the classification of various eye illnesses, fundus images from publically accessible datasets should be subjected to inter-rater reliability testing conducted by both local specialists and the experts employed by such databases. In order to classify fundus photos with difficult and noisy data, we tested deep neural networks. Using 10-fold cross-validation, our suggested approach obtained 85.79% accuracy from the STRESS dataset within a 50-layer ResNet architecture. This four-class eye illness classifier, when using our data preprocessing technique, had a peak accuracy of 91.16%.

In summary, our study showed that, with adjustments to the preprocessing and data gathering phases, multi-category classification applied to public datasets might achieve a notable improvement in performance over earlier studies. Furthermore, this study demonstrated that multiple category diagnosis on various pooled datasets is feasible. Therefore, this can be considered a successful pilot research of classification for the three most prevalent eye diseases in order to create future medical diagnostic helpful tools. We further indicate that researchers planning to use computer-aided techniques for the identification of eye diseases may find inspiration in the publicly available fundus picture databases.

References

[1] . M. A. El-Asrar, "Role of inflammation in the pathogenesis of diabetic retinopathy," Middle East African Journal of Ophthalmology, vol. 19, no. 1, pp. 70–74, 2012.

[2] . [2] S. E. Moss, R. Klein and B. E. K. Klein, "The incidence of vision loss in a diabetic population," Ophthalmology, vol. 95, no. 10, pp. 1340–1348, 1988.

[3] . [3] J. Nayak, P. S. Bhat, U. R. Acharya, C. M. Lim and M. Kagathi, "Automated identification of diabetic retinopathy stages using digital fundus images," Journal of Medical Systems, vol. 32, no. 2, pp. 107–115, 2008.

[4] . L. Verma, G. Prakash and H. K. Tewari, "Diabetic retinopathy: Time for action, no complacency please!," Bulletin of the World Health Organization, vol. 80, no. 5, pp. 419, 2002.

[5] . A. W. Reza and C. Eswaran, "A decision support system for automatic screening of non-proliferative diabetic retinopathy," Journal of Medical Systems, vol. 35, no. 1, pp. 17–24, 2011.

[6] . [6] S. Wild, G. Roglic, A. Green, R. Sicree and H. King, "Global prevalence of diabetes: Estimates for the year 2000 and projections for 2030," Diabetes Care, vol. 27, no. 5, pp. 1047–1053, 2004.

[7] . R. Klein, B. E. K. Klein and S. E. Moss, "The wisconsin epidemiological study of diabetic retinopathy: A review," Diabetes/Metabolism Reviews, vol. 5, no. 7, pp. 559–570, 1989.

[8] . R. Klein, S. M. Meuer, S. E. Moss and B. E. K. Klein, "Retinal microaneurysm counts and 10-year progression of diabetic retinopathy," Archives of Ophthalmology, vol. 113, no. 11, pp. 1386–1391, 1995.

[9] . K. H. Yoon, J. H. Lee, J. W. Kim, J. H. Cho, Y. H. Choi et al., "Epidemic obesity and type 2 diabetes in Asia," The Lancet, vol. 368, no. 9548, pp. 1681–1688, 2006.

[10] . [H. A. Quigley, "Number of people with glaucoma worldwide," British Journal of Ophthalmology, vol. 80, no. 5, pp. 389–393, 1996.

[11] . H. Quigley and A. T. Broman, "The number of people with glaucoma worldwide in 2010 and 2020," British Journal of Ophthalmology, vol. 90, no. 3, pp. 262–267, 2006.

[12] . D. S. Friedman, B. J. O'Colmain, B. Munoz, S. C. Tomany, C. McCarty et al., "Prevalence of age-related macular degeneration in the United States," Archives of Ophthalmology, vol. 122, no. 4,pp. 564–572, 2004.

[13] . C. G. Owen, A. E. Fletcher, M. Donoghue and A. R. Rudnicka, "How big is the burden of visual loss caused by age related macular degeneration in the United Kingdom?," British Journal of Ophthalmology, vol. 87, no. 3, pp. 312–317, 2003.

[14] . R. Kawasaki, M. Yasuda, S. J. Song, S. J. Chen, J. B. Jonas et al., "The prevalence of age-related macular degeneration in Asians: A systematic review and meta-analysis," Ophthalmology, vol. 117, no. 5, pp. 921–927, 2010.

[15] . K. J. Cruickshanks, R. F. Hamman, R. Klein, D. M. Nondahl and S. M. Shetterly, "The prevalence of age-related maculopathy by geographic region and ethnicity: The Colorado-Wisconsin study of age-related maculopathy," Archives of Ophthalmology, vol. 115, no. 2, pp. 242–250, 1997.

[16] . P. Mitchell, W. Smith, K. Attebo and J. J. Wang, "Prevalence of age-related maculopathy in Australia: The Blue Mountains eye study," Ophthalmology, vol. 102, no. 10, pp. 1450–1460, 1995.

[17] . J. S. Sunness, A. Ifrah, R. Wolf, C. A. Applegate and J. R. Sparrow, "Abnormal visual function outside the area of atrophy defined by short-wavelength fundus autofluorescence in Stargardt disease," Investigative Ophthalmology and Visual Science, vol. 61, no. 4, pp. 36, 2020.

[18] . R. Klein, K. J. Cruickshanks, S. D. Nash, E. M. Krantz, F. J. Nieto et al., "The prevalence of age-related macular degeneration and associated risk factors," Archives of Ophthalmology, vol. 128, no. 6, pp. 750–758, 2010.

[19] . T. Wong, U. Chakravarthy, R. Klein, P. Mitchell, G. Zlateva et al., "The natural history and prog-nosis of neovascular age-related macular degeneration: A systematic review of the literature and meta-analysis," Ophthalmology, vol. 115, no. 1, pp. 116–126.e1, 2008.

[20] . W. L. Wong, X. Su, X. Li, C. M. G. Cheung, R. Klein et al., "Global prevalence of age-related macular degeneration and disease burden projection for 2020 and 2040: A systematic review and meta-analysis," The Lancet Global Health, vol. 2, no. 2, pp. e106–e116, 2014.

[21] . T. S. Hwang, Y. Jia, S. S. Gao, S. T. Bailey, A. K. Lauer et al., "Optical coherence tomog-raphy angiography features of diabetic retinopathy," Retina (Philadelphia, Pa.), vol. 35, no. 11,pp. 2371–2376, 2015.

[22] . I. I. Bussel, G. Wollstein and J. S. Schuman, "OCT for glaucoma diagnosis, screening and detection of glaucoma progression," British Journal of Ophthalmology, vol. 98, no. Suppl. 2, pp. ii15–ii19, 2014.

[23] . C. S. Lee, D. M. Baughman and A. Y. Lee, "Deep learning is effective for classifying normal versus age-related macular degeneration OCT images," Ophthalmology Retina, vol. 1, no. 4, pp. 322–327, 2017.

[24] . S. Qummar, F. G. Khan, S. Shah, A. Khan, S. Shamshirband et al., "A deep learning ensemble approach for diabetic retinopathy detection," IEEE Access, vol. 7, pp. 150530–150539, 2019.

[25] . M. Mateen, J. Wen, S. S. Nasrullah and Z. Huang, "Fundus image classification using VGG-19 architecture with PCA and SVD," Symmetry, vol. 11, no. 1, pp. 1, 2018.

[26] . A. Singh, M. K. Dutta, M. ParthaSarathi, V. Uher and R. Burget, "Image processing based automatic diagnosis of glaucoma using wavelet features of segmented optic disc from fundus image," Computer Methods and Programs in Biomedicine, vol. 124, pp. 108–120, 2016.

[27] . J. H. Tan, S. V. Bhandary, S. Sivaprasad, Y. Hagiwara, A. Bagchi et al., "Age-related macular degeneration detection using deep convolutional neural network," Future Generation Computer Systems, vol. 87, pp. 127–135, 2018.

[28] . G. G. Gardner, D. Keating, T. H. Williamson and A. T. Elliott, "Automatic detection of diabetic retinopathy using an artificial neural network: A screening tool," British Journal of Ophthalmology, vol. 80, no. 11, pp. 940–944, 1996.

[29] . R. Banu, V. Arun, N. Shankaraiah and V. Shyam, “Meta-cognitive neural network method for classification of diabetic retinal images,” in Proc. 2nd Int. Conf. on Cognitive Computing and Information Processing.
[30] . U. Raghavendra, S. V. Bhandary, A. Gudigar and U. R. Acharya, “Novel expert system for glau-coma identification using non-parametric spatial envelope energy spectrum with fundus images,” Biocybernetics and Biomedical Engineering, vol. 38, no. 1, pp. 170–180, 2018.
[31] . U. Raghavendra, H. Fujita, S. V. Bhandary, A. Gudigar, J. H. Tan et al., “Deep convolution neural network for accurate diagnosis of glaucoma using digital fundus images,” Information Sciences, vol. 441, pp. 41–49, 2018.
[32] . P. Burlina, D. E. Freund, N. Joshi, Y. Wolfson and N. M. Bressler, “Detection of age-related macular degeneration via deep learning,” in Proc. 13th IEEE Int. Sym. on Biomedical Imaging (ISBI), Prague,Czech Republic, pp. 184–188, 2016.
[33] . J. Y. Choi, T. K. Yoo, J. G. Seo, J. Kwak, T. T. Um et al., “Multi-categorical deep learning neural network to classify retinal images: a pilot study employing small database,” PLoS One, vol. 12, no. 11, e0187336, 2017.
[34] . Z. Zhang, F. S. Yin, J. Liu, W. K. Wong, N. M. Tan et al., “ORIGA-light: An online retinal fundus image database for glaucoma analysis and research,” in Proc. 2010 Annual Int. Conf. of the IEEE Engineering in Medicine and Biology, EMBC’10, Buenos Aires, Argentina, pp. 3065–3068, 2010.
[35] . P. Porwal, S. Pachade, R. Kamble, M. Kokare, G. Deshmukh et al., “Indian diabetic retinopathy image dataset (IDRiD): A database for diabetic retinopathy screening research,” Data, vol. 3, no. 3,pp. 25, 2018.
[36] . E. Decencière, X. Zhang, G. Cazuguel, B. Lay, B. Cochener et al., “Feedback on a publicly distributed image database: The Messidor database,” Image Analysis and Stereology, vol. 33, no. 3, pp. 231–234, 2014.
[37] . Y. Zheng, M. H. A. Hijazi and F. Coenen, “Automated ‘disease/no disease’ grading of age-related macular degeneration by an image mining approach,” Investigative Opthalmology and Visual Science,vol. 53, no. 13, pp. 8310–8318, 2012.
[38] . D. J. J. Farnell, F. N. Hatfield, P. Knox, M. Reakes, S. Spencer et al., “Enhancement of blood vessels in digital fundus photographs via the application of multiscale line operators,” Journal of the Franklin Institute, vol. 345, no. 7, pp. 748–765, 2008.
[39] . A. Hoover, “Locating blood vessels in retinal images by piecewise threshold probing of a matched filter response,” IEEE Transactions on Medical Imaging, vol. 19, no. 3, pp. 203–210, 2000.
[40] . A. Hoover and M. Goldbaum, “Locating the optic nerve in a retinal image using the fuzzy convergence of the blood vessels,” IEEE Transactions on Medical Imaging, vol. 22, no. 8, pp. 951–958, 2003.
[41] . J. H. Han, S. Yang and B. U. Lee, “A novel 3-D color histogram equalization method with uniform 1-D gray scale histogram,” IEEE Transactions on Image Processing, vol. 20, no. 2, pp. 506–512, 2011.
[42] . D. Menotti, L. Najman, A. De A. Arájo and J. Facon, “A fast hue-preserving histogram equalization method for color image enhancement using a Bayesian framework,” in Proc. 14th Int. Workshop on Systems, Signals and Image Processing, and 6th EURASIP Conf. Focused on Speech and Image Processing,Multimedia Communications and Services, Maribor, Slovenia, pp. 414–417, 2007.
[43] . S. K. Naik and C. A. Murthy, “Hue-preserving color image enhancement without gamut problem,” IEEE Transactions on Image Processing, vol. 12, no. 12, pp. 1591–1598, 2003.
[44] . G. Bradski and A. Kaehler, “Learning OpenCV: Computer vision with the OpenCV library,” in Computer Vision with the OpenCV Library, California, USA: O’Reilly Media, Inc., 2008.
[45] . L. Breiman and P. Spector, “Submodel selection and evaluation in regression, the X-random case,” International Statistical Review/Revue Internationale de Statistique, vol. 60, no. 3, pp. 291, 1992.
[46] . R. Kohavi, “A study of cross-validation and bootstrap for accuracy estimation and model selection,” Ijcai, vol. 14, no. 2, pp. 1137–1145, 1995.
[47] . S. Ruder, “An overview of gradient descent optimization algorithms.” arXiv preprint arXiv: 1609. 04747, 2016.
[48] . E.Rezende, G. Ruppert, T. Carvalho, F. Ramos and P. De Geus, “Malicious software classification using transfer learning of ResNet-50 deep neural network,” in Proc. 16th IEEE Int. Conf. on Machine Learning and Applications (ICMLA), Cancún, Mexico, pp. 1011–1014, 2017.
[49] . K. He, X. Zhang, S. Ren and J. Sun, “Deep residual learning for image recognition,” in Proc. 2016 IEEE Conf. on Computer Vision and Pattern Recognition, Nevada, USA, pp. 770–778,
[50] . K. Simonyan and A. Zisserman, “Very deep convolutional networks for large-scale image recognition.” arXiv preprint arXiv: 1409. 1556, 1–14, 2014.
[51] . M. D. Zeiler, “Adadelta: An adaptive learning rate method.” arXiv preprint arXiv: 1212. 5701, 2012.
[52] . Y. Gal and Z. Ghahramani, “A theoretically grounded application of dropout in recurrent neural networks,” in 30th Conf. on Neural Information Processing Systems, Barcelona, Spain, pp. 1019–1027,2016.
[53] . M. Abadi, A. Agarwal, P. Barham, E. Brevdo, Z. Chen et al., “TensorFlow: Large-scale machine learning on heterogeneous distributed systems,” arXiv preprint arXiv: 1603. 04467, 2016.
[54] . F. Pedregosa, G. Varoquaux, A. Gramfort, V. Michel, B. Thirion et al., “Scikit-learn: Machine learning in Python,” The Journal of Machine Learning Research, vol. 12, pp. 2825–2830, 2011.
[55] . L. Perez and J. Wang, “The effectiveness of data augmentation in image classification using deep learning.” arXiv preprint arXiv: 1712. 04621, 2017.